How to cite: *Angew. Chem. Int. Ed.* **2024**, *63*, e202315326
doi.org/10.1002/anie.202315326

Polymer Chemistry | Hot Paper

Ambient Catalytic Spinning of Polyethylene Nanofibers

Ruikai Wu, Tim M. Lenz, Fayez Abdullah S Alfayez, Ruohan Zhao, Patrick Rupper, Edith Perret, Sandro Lehner, Milijana Jovic, Sabyasachi Gaan, Bernhard Rieger, and Manfred Heuberger**

Abstract: A novel single-atom Ni(II) catalyst (**Ni-OH**) is covalently immobilized onto the nano-channels of mesoporous Santa Barbara Amorphous (SBA)-15 particles and isotropic Anodized Aluminum Oxide (AAO) membrane for confined-space ethylene extrusion polymerization. The presence of surface-tethered Ni complexes (**Ni@SBA-15** and **Ni@AAO**) is confirmed by the inductively coupled plasma-optical emission spectrometry (ICP-OES) and X-ray photoelectron spectroscopy (XPS). In the catalytic spinning process, the produced PE materials exhibit very homogeneous fibrous morphology at nanoscale (diameter: ~50 nm). The synthesized PE nanofibers extrude in a highly oriented manner from the nano-reactors at ambient temperature. Remarkably high M_w (1.62×10^6 g mol^{-1}), melting point (124 °C), and crystallinity (41.8 %) are observed among PE samples thanks to the confined-space polymerization. The chain-walking behavior of surface tethered Ni catalysts is greatly limited by the confinement inside the nano-channels, leading to the formation of very low-branched PE materials (13.6/1000 C). Due to fixed supported catalytic topology and room temperature, the filaments are expected to be free of entanglement. This work signifies an important step towards the realization of a continuous mild catalytic-spinning (CATSPIN) process, where the polymer is directly synthesized into fiber shape at negligible chain branching and elegantly avoiding common limitations like thermal degradation or molecular entanglement.

Introduction

Fibers and fibrous materials are widely used, e.g. in the textile and apparel industry.[1] Different spinning techniques (naturally or artificially) for fibers exist.[2] For example, protein-based silk from spiders and other glanded animals exhibits remarkable mechanical performance, which can readily exceed the strength of steel and suggests that the spinning process is key.[3,4] Nowadays, synthetic fabric materials constitute the bulk volume of products made of polymers like polyester, polyamide, polyolefin, and polyacrylonitrile.[5] While synthetic fibers exhibit remarkable and reproducible properties, the current manufacturing procedures (i.e. melt-spinning or wet-spinning) involve energy and resources intensive processes. They really work only for a small selection of polymers and are thus still far away from competing with gentle bio-based equivalents.[6] In a notably unique report, Aida and his co-workers pioneered ethylene extrusion polymerization near ambient temperature using the titanocene complexes immobilized on mesoporous silica.[7]

Catalysis has become an indispensable tool to enable and control the polymerization process ever since *Ziegler* and *Natta* won the Nobel Prize in Chemistry for their discovery of heterogeneous catalysts applied to olefin polymerization.[8] The field of coordination-insertion polymerization has seen a long span of prosperity in both academia and industry.[9] Heterogeneous catalysts exhibit great advantages in thermal stability, yield, polymeric morphology control and producing low contamination to the reactor. However, they also come with drawbacks like low efficiency of the catalytic initiation process, broad molecular weight distributions and limited mechanical properties of produced polymers.[8c] With the advent of late-transition complexes for olefin polymerization, single-site catalysts are

[*] R. Wu, F. A. S Alfayez, R. Zhao, Dr. P. Rupper, Dr. E. Perret, S. Lehner, M. Jovic, Dr. S. Gaan, Prof. Dr. M. Heuberger
Laboratory of Advanced Fibers
Empa, Swiss Federal Laboratories for Materials Science and Technology
Lerchenfeldstrasse 5, 9014 St. Gallen, Switzerland
E-mail: Manfred.Heuberger@empa.ch
sabyasachi.gaan@empa.ch

R. Wu, Prof. Dr. M. Heuberger
Department of Materials
ETH Zurich
8092 Zurich, Switzerland

T. M. Lenz, Prof. Dr. B. Rieger
WACKER-Chair of Macromolecular Chemistry
Catalysis Research Center, Technical University of Munich
Lichtenbergstraße 4, 85748 Garching, Germany

now appearing as viable alternative to modern catalysts.[10] In ethylene (co)polymerization, the Ni complexes with NN-chelating (α-diimine) ligands exhibit remarkable catalytic performance and capacity in controlling the PE microstructures via the so-called chain-walking process.[11] Unique and functional polymers with superb mechanical properties, such as ultrahigh molecular weight PE and highly branched elastomeric polymers can be synthesized using ethylene as the main reactive monomer. The successful immobilization of such late-transition-metal complexes could bring the present academic research to the level of future industrial applications.[12]

Here, we present progress in the direction of novel catalytic-spinning strategy, which should allow one to obtain PE nano-fibers directly from the ethylene monomer (Figure 1). Namely, we investigate the ethylene extrusion polymerization from mesoporous particles and membrane perforated with nano-channels. Covalently tethered α-diimine Ni complex (**Ni-OH**) decorate the inner surface of pores that serve as the nano-reactors for confined-space ethylene polymerization. The polymer microstructure is expected to be significantly different compared to the conventional process involving homogeneous polymerization followed by melt processing. The confined-space effects inside the nano-pores provide a unique coordination environment for monomer insertion and chain-walking processes of such Ni-based heterogeneous single-atom catalysts (SAC). Surface-confinement protects the coordination-insertion process from chain transfer and termination; the former followed by β-hydrogen reinsertion leads to the formation of branching structures in PE.

Results and Discussion

Ethylene extrusion polymerization catalyzed by Ni@SBA-15

The mesoporous materials with uniform porous dimensions, like MSM-41(Mobil Composition of Matter No. 41) and SBA-15 silica, are of great interest due to their potential applications in catalysts and/or catalyst supports for chemical synthesis.[13] Previously, Aida and his co-workers reported the production of crystalline polyethylene fibers by the ethylene extrusion polymerization using the titanocene complexes immobilized on mesoporous silica.[7] Based on the recent development of late-transition metal complexes for olefin polymerization and mesoporous materials, we have performed a confined-space ethylene extrusion polymerization by SBA-15 supported α-diimine Ni complex (**Ni@SBA-15**).[14] This approach allows the tunable control of both catalytic performances of **Ni-OH** and isolated PE microstructures in ethylene heterogeneous polymerization.

Subsequently, the ethylene polymerization catalyzed by **Ni@SBA-15** was initially carried out at 2 bar and different temperatures (Table 1). A parallel set of **Ni-OH-**catalyzed ethylene polymerization was also performed for comparison study (Table S1). In Figure 2a, it is observed that both the PE M_w and catalytic activity of Ni complexes gradually decrease from 20 to 80 °C. High catalytic activity (5.6×10^5 g of PE (mol of Ni)$^{-1}$ h^{-1}) and ultrahigh molecular weight (1.53×10^6 g mol^{-1}) can be achieved at 10 bar and 30 °C. The PE M_w observed in confined-space polymerization is significantly higher than the one in general homogeneous polymerization. **Ni@SBA-15** represents a single-site catalyst in such heterogeneous polymerization (Figure S1).

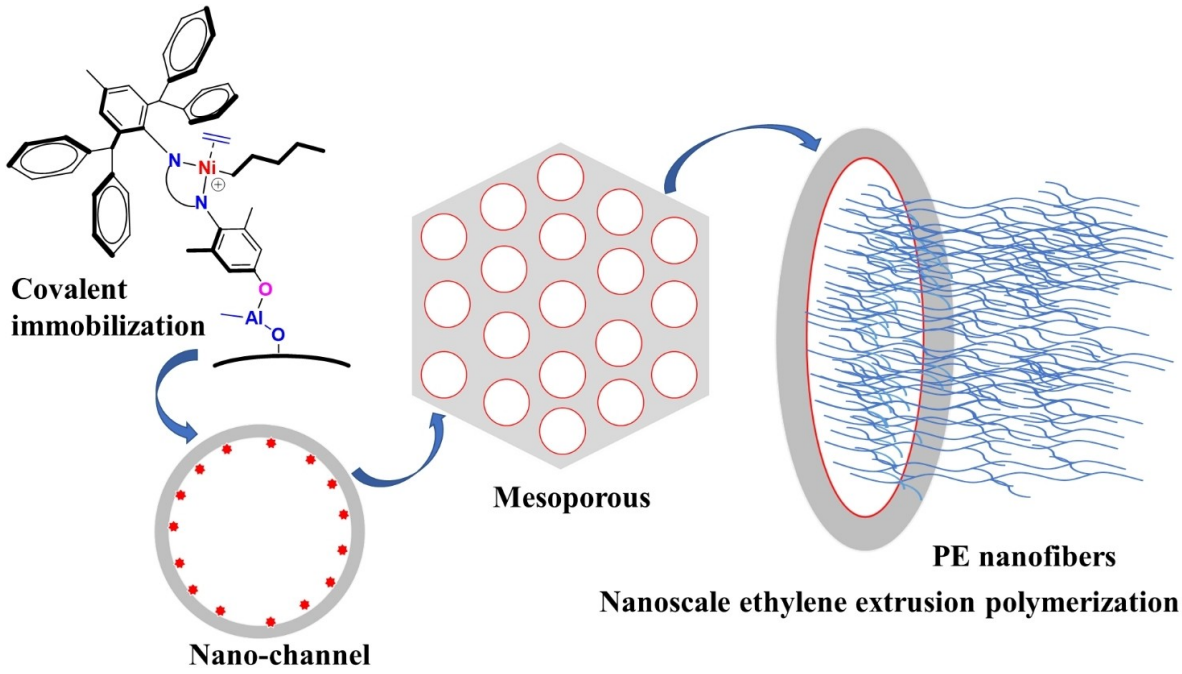

Figure 1. Ethylene confined-space polymerization in the nano-channels of SBA-15/AAO catalyzed by the covalently tethered α-diimine Ni complex (**Ni-OH**).

Table 1: Ethylene slurry-phase polymerization with SBA15-supported **Ni-OH**.[a]

Entry	Ni	P, bar	T, °C	t, min	Yield, g	Act.[b]	M_w[c]	M_w/M_n[c]	B/1000C[d]	T_m[e], °C
1	**Ni@SBA-15**	2	20	60	1.69	1.69	0.79	3.9	67.3	120.3
2	**Ni@SBA-15**	2	30	60	2.50	2.50	0.67	2.3	69.4	50.9
3	**Ni@SBA-15**	2	40	60	2.65	2.65	0.61	3.0	69.6	36.4
4	**Ni@SBA-15**	2	60	60	2.04	2.04	0.35	2.6	79.6	-
5	**Ni@SBA-15**	2	80	60	1.33	1.33	0.23	4.0	86.8	-
6	**Ni@SBA-15**	10	30	60	5.69	5.69	1.53	2.3	33.4	82.3

[a] General conditions for ethylene polymerization: 10 μmol of **Ni@SBA-15** precatalysts; cocatalyst: EASC; Al/Ni = 500; 100 mL total volume of anhydrous toluene; 3000 r/min. [b] Unit of 10^5 g of PE (mol of Ni)$^{-1}$ h^{-1}. [c] Unit of 10^6 g mol^{-1}, determined by GPC in 1,2,4-trichlorobenzene at 160 °C versus linear polystyrene standards. [d] Branched density, determined by high-temperature ^{1}H NMR spectra. [e] Determined by DSC (second heating scan).

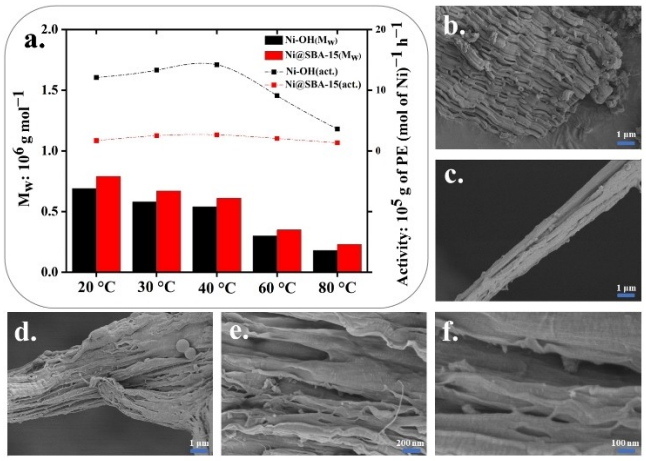

Figure 2. Plot of the comparative study on the Ni catalytic activity/PE M_w catalyzed by **Ni-OH**/**Ni@SBA-15** (a) and SEM images of mesoporous SBA-15 (b)/PE samples (Table 1) synthesized by **Ni@SBA-15**: SEM image of entry 1 (c) and different magnifications of entry 3 (d, e, and f).

In terms of PE morphology, the nanofibrous structures are observed in all PE samples obtained from the ethylene extrusion polymerization. Figure 2b shows the distinctive morphology of **Ni@SBA-15**. It consists of thousands of uniform pores with 6 to 11 nm in diameter, decorated by **Ni-OH** via covalent immobilization and thus serving as the nanoreactor for ethylene polymerization. In addition, a PE multifilament bunch can be seen in Figure 2c, which contains numerous PE nano-fibers at around 50 to 100 nm in diameter. These typical shapes relate to the extrusion polymerization mechanism at nanoscale: with the initiation of Ni catalyst, the polymer chain starts to grow and quickly coils inside the pore to be extruded by the growth of other chains in a following process of mutual alignment. The pressure inside of the nanochamber steadily increases with continued polymerization. The internal pore pressure eventually orientates the polymer growth in an extrusion mode. The nanochannels of **Ni@SBA-15** play the role of both nanoscale reactor and extruder for ethylene polymerization. Extruded nano-filaments then cluster to large bunches via attractive Van der Waals forces.

This general Scheme is evidenced by Figure 2d–f at different magnifications, where a similar observation has been found in the rest of PE samples obtained by the **Ni@SBA-15** catalyzed extrusion polymerization. Moreover, the diameter of PE nanofibers is generally higher than the nominal nano-pore diameter, which implies the possibility of pore overstraining during pressure buildup. As previously observed on substrates, the chain-walking behavior of **Ni@SBA-15** was significantly inhibited by confinements from the nano-channel, which was characterized by high-temperature NMR spectroscopy.[11i] The PE nanofibers exhibit relatively lower branching densities than the PE produced via homogeneous polymerization (Figure S2–S14). Various branching (methyl, ethyl, propyl, butyl, amyl and long-chain) structures are observed by the ^{13}C NMR spectra for the PE sample (entry 6 in Table S1) homogeneously synthesized by **Ni-OH** (Figure S15). Oppositely, only methyl branches are determined from the PE nanofibers (entry 6 in Table 1), which have been obtained from the **Ni@SBA-15** catalyzed extrusion polymerization (Figure S16).

Catalytic-spinning process catalyzed by Ni@AAO

Although mesoporous silica bears large potential in olefin polymerization, only a limited amount of interest is generated in both academia and industry. This may result from a limitation on the applications of mesoporous silica. For instance, the poor mechanical properties of mesoporous silica hardly promises a further chance of confined-space polymerization for mass production and analysis. Based on the powder morphology, it is also very difficult to perform the post-separation of the heterogeneous catalysts after the olefin polymerization. On the contrary, Al alloys and Al_2O_3 ceramics are widely applied in industrial manufacture.[15] Therefore, we have carried out the ethylene polymerization in an isotropic anodized Al_2O_3 (AAO) membrane, which provides a high surface density of nano-channels with a well-defined dimension. The **Ni-OH** catalysts are implanted inside the AAO nanopores via a similar covalent-immobilization strategy to **Ni@SBA-15**, which are ready for the ethylene confined-space polymerization. The produced PE (**PE-AAO**) by **Ni@AAO** however exhibits the distinctive morphology of the nano-fibrous polymer. To further characterize polymerization mechanism and polymeric properties of **PE-AAO**, additional analytic measurements were performed. First, the immobilization process of **Ni-OH** onto the AAO membrane was investigated by X-ray photoelectron spectroscopy (XPS). Five samples were prepared, namely, the **Ni-OH** catalyst, the AAO membrane, the $AlMe_3$-treated AAO membrane, the Ni catalyst on the AAO membrane (**Ni@AAO**) and the produced nanofibrous PE (PE-AAO). Figure 3(a) depicts the survey scans for these five samples. The elements carbon (C), oxygen (O), nickel (Ni), nitrogen (N) and chlorine (Cl) expected for the catalyst molecular structure are clearly observed for **Ni-OH**. The only other

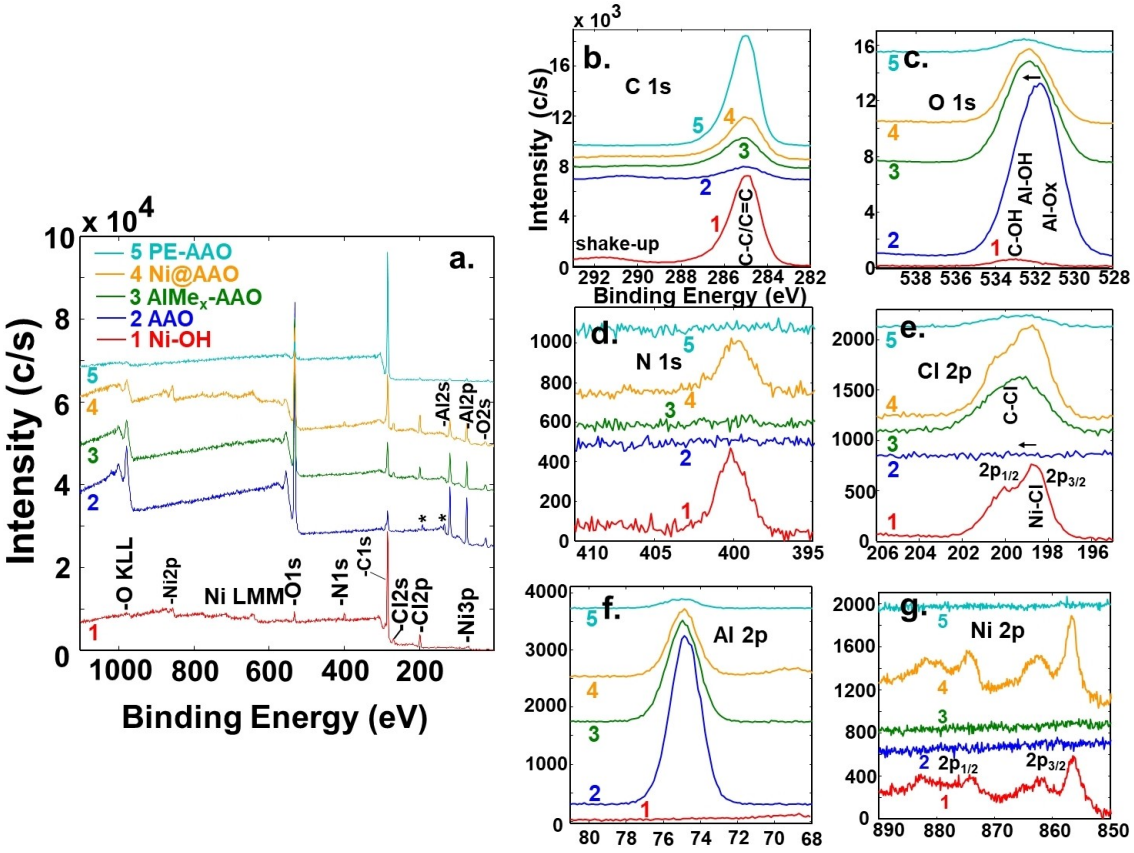

Figure 3. Comparison of XPS spectra of the initial Ni catalyst (**Ni-OH**), the AAO membrane (AAO), the $AlMe_3$-treated AAO membrane ($AlMe_x$-AAO), the Ni catalyst tethered on the AAO membrane (**Ni@AAO**) and the produced nano fibrous PE (PE-AAO). The spectra are offset in the *y*-direction for better visualization. a) Surveys scans with peak labelling (peak positions of phosphorus are marked with asterisks). b) High-resolution scans for C 1s, c) for O 1s, d) for N 1s, e) for Cl 2p, f) for Al 2p and g) for Ni 2p. Arrows depict significant shifts in binding energy due to changed surface chemistry (see text for details).

sample with a presence of Ni and N was **Ni@AAO**, indicating the successful attachment of the catalyst on the supporting AAO membrane. Considering an information depth of XPS of about 5 nm by assuming an inelastic mean free path of $\lambda = 2.2$ nm, the sensitivity was not possible to detect Ni and N from the catalyst below the polyethylene layer (a couple of nm's thick) for the PE-AAO sample.[16] All samples containing the aluminum oxide membrane show, as expected, an additional Al signal. In the PE-AAO sample, the Al signal intensity was significantly reduced, again due to the polyethylene layer attenuating photoelectrons from the substrate. Small impurities of phosphorus (<2 atomic %) were found on the aluminum oxide membrane (produced by phosphoric acid corrosion), but the signal vanished below detection limit after treating and washing the membrane.

High-resolution elemental scans were also measured to characterize the oxidation states of chemical bonds (see Figures 3b) to g)). For the pure **Ni-OH** catalyst, the C 1s spectrum (Figure 3b) shows a strong C=C peak at 285 eV (internal reference) from the phenyl rings in the molecular structure. There is a smaller π–π* bond shakeup peak at 291.5 eV, which is a common energy-loss feature of aromatic carbon species.[17] The O 1s peak at 533.1 eV (Figure 3c) is typical for a C–OH group, the N 1s peak at 400.1 eV (Figure 3d) represents organic nitrogen and the Cl $2p_{3/2}$ spin-orbit component at 198.7 eV (Figure 3e) is characteristic for nickel chloride–all in agreement with the known molecular structure of the catalyst.[18] The Ni $2p_{3/2}$ band was fitted using literature data from Biesinger and co-workers, who have studied and fitted several reference Ni oxides and halides offering a complex structure resulting from multiplet splitting as well as shake-up and plasmon loss structures.[19] The binding energies of the main peak around 856.6 eV and the satellite peak at 862.3 eV (see Figure 3 g) agree well with $NiCl_2$. In order to remove potentially physisorbed catalyst molecules, the **Ni@AAO** sample was thoroughly washed in dichloromethane by ultrasonic cleaner before measuring. No significant change in the chemical bonding environment was observed between Ni in the pure catalyst (**Ni-OH**) and the catalyst bonded to the aluminum oxide membrane (**Ni@AAO**) (see Figure 3 g). In addition, the nitrogen and chlorine signals are very similar (position, intensity) in-between these two samples, proving the intact coordination at the catalytic Ni center and showing that the covalent immobilization reaction, as intended, mainly takes place between the functionalized AAO membrane and the hydroxyl group from the **Ni-OH** catalyst. A successful

treatment of the AAO membrane as preparation to immobilize the catalyst was also confirmed by XPS. The reference AAO membrane surface exhibits a mixture of aluminum oxide and hydroxide, while a clear binding energy shift was observed after the treatment with trimethylaluminum, (see Figure 3c) due to a changed surface with additional Al-O–Al$(CH_3)_x$ groups. No significant change in the Al 2p band was observed (see Figure 3f), which is expected because the binding energy shifts for various Al states are small.[20] Some physisorbed solvent (dichloromethane) was evidenced on the treated AAO sample (see Figure 3e), as observed from the chlorine signal (C–Cl) that clearly shifted towards higher binding energies compared to the signal from Ni–Cl. Finally, the sample of PE-AAO obtained from ethylene extrusion polymerization exhibited predominantly C–C aliphatic bonds at 285.0 eV, with a minor presence of Al and O originating from the underlying substrate membrane.[21]

After polymerization, the PE nanofibers (PE-AAO) microstructures can be characterized. As shown in Figure 4a, the AAO membrane consists of well-defined nano-pores. The uniform pore structure (pore diameter: 50 nm) across the membrane thickness (50 μm) connects pore openings on both sides of the AAO membrane, making them an ideal supporting substrate for the confined-space polymerization that could be operated continuously in one flow direction in future. The extrusion polymerization catalyzed by **Ni@AAO** is active inside the pores of the AAO membrane, which serve as the nano-reactors. To compare results, the polymerization conditions are set to entry 6 in Table 1 (and Table S1). We note that the activity seen with **Ni@AAO** is lower than the activity of the homogeneous polymerization catalyzed by **Ni-OH**; this is due to a limited Ni catalysts surface density as well as a self-limited ethylene monomer diffusion into the AAO pores. In order to produce/collect enough PE for further analysis, the confined-space polymerization proceeds 10 hours after the initiation of ethylaluminum sesquichloride (EASC) as co-catalyst. After ethylene polymerization, the morphology of the PE-AAO sample is investigated with scanning electron microscopy (SEM). In Figure 4b, numerous rope-like polymer bunches extend from the top surface of the AAO membrane. Further out,

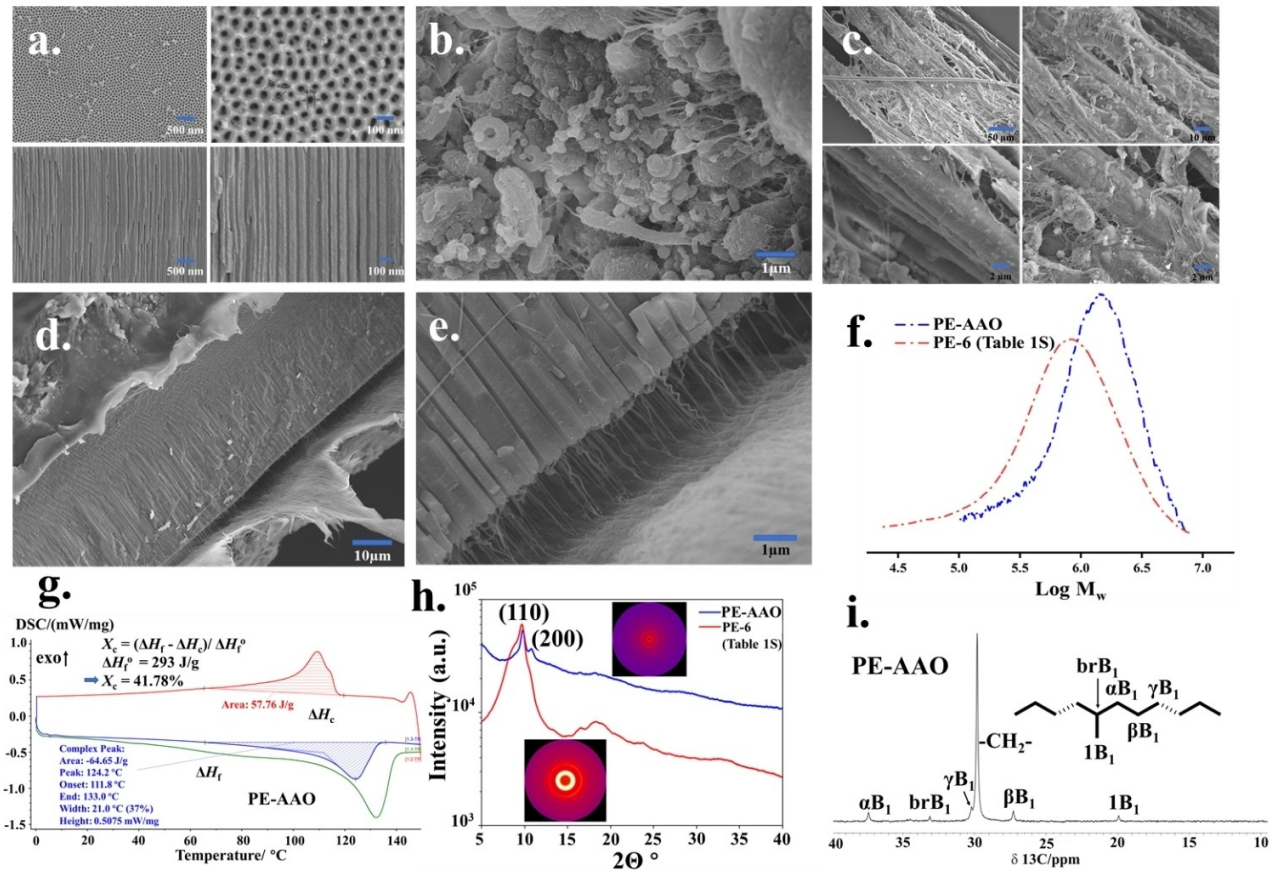

Figure 4. SEM images and microstructures of PE-AAO after extrusion polymerization; (a) SEM image of supporting AAO membrane top surface and cross section at different magnifications; (b) SEM image of PE-AAO top surface obtained using **Ni@AAO** in toluene; (c) SEM image of collected polymer sample from the PE-AAO top surface under different magnifications; (d) SEM image of PE-AAO cross section obtained using **Ni@AAO** in toluene; (e) enlarged magnification of image (d); (f) GPC traces of the PE-AAO and PE-6 (Table S1) as measured by High-temperature GPC in 1,2,4-trichlorobenzene at 160 °C; (g) Melting behavior and crystallinity of PE-AAO as derived from DSC data obtained at a heating rate of 10 °C/min; (h) Wide-angle X-ray diffraction (WAXD) spectra and 2D WAXD patterns of PE-AAO and PE-6 (Table S1); (i) High-temperature ^{13}C NMR spectra of PE-AAO in Bromobenzene-d_5.

the produced PE forms a thin polymeric microfilm, presumably owing to the presence of toluene. Although mesoporous materials contains extremely high internal surface areas, theoretically, there is trace amount of Ni catalyst remaining on the top surface of the AAO membrane, caused by the homogeneous immobilization process of **Ni-OH** onto AAO samples. The polymer on the AAO top surface was removed and characterized by SEM. As shown in Figure 4c, all the PE samples exhibit a uniformly oriented fibrous structures. It indicates that most of the PE nanofibers indeed extrude from the AAO nano-channels. It is worth noting that the diameters of the PE fibers are larger than the AAO pore size (50 nm). There seems to be a trend that individual nano-fibrils naturally intertwined into bunches.

The post-polymerization morphology analysis of the PE-AAO cross section reveals that the AAO membrane is covered by the PE fibers on both sides (Figure 4d). Moreover, distinctive fibrous structures are observed that are reminiscent of an extrudate from the nano-reactors in the AAO membrane. At higher magnification, (see Figure 4e) this statement is confirmed; i.e. single polymeric nano-fibers are extruded out of individual AAO nano-channels and bunch up to form an accumulated PE polymeric fiber at macroscopic scales. The diameter of the individual PE nanofibers matches the diameter of the AAO nano-pores and the AAO membrane remains intact despite an expected internal pressure buildup. The polymeric chain growth is at room temperature and oriented inside a confining pore; together with the fact that the catalytic centers are tethered to fixed positions at the pore walls, the extruded nano-fibers is expected to be free of entanglement. These results are very promising and bear the potential for a novel catalytic spinning technology, where monomers from one side are polymerized into fibers across a catalytic nano-porous membrane. Another advantage of such process is that the product can be free of catalyst. Today, the separation catalysts from the produced polyolefins is still a complicated procedure.[22] Compared to our reference PE-6 in **Ni-OH** catalyzed homogeneous polymerization (entry 6 in Table S1), the **Ni@AAO** also exhibits a similar single-atom catalytic behavior based on the GPC traces of the PE-AAO (Figure 4f). Meanwhile, the PE-AAO (1.62×10^6 g mol^{-1}) synthesized by the **Ni@AAO** catalyzed confined-space ethylene polymerization exhibits a higher molecular weight (M_w) than the PE-6 (1.07×10^6 g mol^{-1}) reference sample in Table S1. As widely accepted, the Ni catalyzed ethylene polymerization produces a highly branched PE with multiple types of branching structures (methyl, ethylene…, and longer branches).[23] This leads to nearly amorphous polymer properties including low melting point, as confirms the PE-6 reference. Remarkably, PE-AAO polymerized in confined-space geometry exhibits a significantly higher melting point (124 °C) and crystallinity ($X_c = 41.8\,\%$) that the PE-6 reference in Table S1, as measured by DSC and illustrated in Figure 4g. The Wide-angle X-ray diffraction (WAXD) analysis also confirms the DSC results. PE-6 has indeed a high amorphous content, where the preferred distances between neighboring molecules are in the range of 4.5 Å. The WAXD pattern of PE-AAO shows however sharp crystalline rings and a lower amorphous contribution (Figure 4h). It indicates that the orientation of the polymer chain in PE-AAO significantly higher than the one in PE-6, which is potentially caused by the effects of confined-space polymerization and polymer extrusion from AAO nano-reactors. Additionally, the PE branching densities and structures in Ni catalyzed polymerization are mainly modulated by the β-H elimination and reinsertion, also known as chain-walking process.[11] Due to the covalent immobilization of catalytic Ni center on the supporting substrates, the confinement introduced by the nanopores of the AAO substrates restricts the free rotation of N-aryl groups and thus β-H reinsertion at equilibrium;causing this poses effective steric restrictions on the chain-walking process and PE branches formation. As shown in Figure 4i, only methyl branching is determined in the PE-AAO sample by the ^{13}C HTNMR . In addition, the branching density of the PE-AAO (13.6 BD/1000 C in Figure S17) from confined **Ni@AAO** polymerization is much lower than the one of the PE-6 reference sample (76.3 % in Figure S8). Along these lines we note that similar control of branching is state of the art, but through laborious organic ligand modifications of the precursors of the Ni complexes.[11d,24]

Conclusions

In conclusion, we demonstrated that the extrusion polymerization reported by Aida et al. works on different kinds of nano pores with novel Ni-based catalysts. The process can be parallelized utilizing membranes with many nano-pores in parallel. This is understood as an important step towards a novel promising catalytic-spinning (CATSPIN) technique either from mesoporous SBA-15 nanoparticles or across an AAO membrane. The process takes place at room temperature and yields polymeric fibrils with remarkable properties like high molecular weight, high melting point, low branching, and high crystallinity in line with the expected absence of entanglement. In addition, the covalently immobilized Ni(II) complexes (**Ni@SBA**/**Ni@AAO**) exhibit more efficient catalytic performance in the confined-space polymerization than the one (**Ni-OH**) in the solution-phase polymerization. The confinement effects modulate the chain-growth and chain-walking process during the ethylene polymerization. More generally, a finely controlled chain-walking behavior of late-transition metal catalysts via confinement indicates a promising alternative to the current olefin catalysts for commercial application in industry. In near future, we see room to explore the here demonstrated multifilament catalytic-spinning technique in a continuous-directional reactor and involving other catalysts and polymer families.

Supporting Information

The authors have cited additional references within the Supporting Information (Ref. [14,25]).

Acknowledgements

This work was financially supported by SwissTextiles and the Subitex platform (2020–2025) as well as the China Scholarships Council (No. 201904910562). Open Access funding provided by ETH-Bereich Forschungsanstalten.

Conflict of Interest

The authors declare no conflict of interest.

Data Availability Statement

The data that support the findings of this study are available from the corresponding author upon reasonable request.

Keywords: Ni (II) complex · confined-space polymerization · inhibited chain-walking behavior · PE nanofibers · high molecular weight

[1] a) H. Bao, Y. Hong, T. Yan, X. Xie, X. Zeng, *J. Text. Inst.* **2023**, 1–20; b) P. S. Deora, M. Khurana, R. A. Muhal, D. Upadhyay, C. Goswami, *Mater. Today: Proc.* **2022**, *60*, 2230–2235.
[2] Z. Xu, M. Wu, Q. Ye, D. Chen, K. Liu, H. Bai, *Engineering* **2022**, *14*, 100–112.
[3] S.-M. Lee, E. Pippel, U. Gösele, C. Dresbach, Y. Qin, C. V. Chandran, T. Bräuniger, G. Hause, M. Knez, *Science* **2009**, *324*, 488–492.
[4] S. K. Ramamoorthy, M. Skrifvars, A. Persson, *Polym. Rev.* **2015**, *55*, 107–162.
[5] G. Bhat, V. Kandagor, *Advances in filament yarn spinning of textiles and polymers*, Elsevier, **2014**, pp. 3–30.
[6] J. Song, M. Kim, H. Lee, *Polymer* **2020**, *12*, 1386.
[7] a) K. Kageyama, J.-i. Tamazawa, T. Aida, *Science* **1999**, *285*, 2113–2115; b) P. Lehmus, B. Rieger, *Science* **1999**, *285*, 2081–2082.
[8] a) C. Vogt, B. M. Weckhuysen, *Nat. Chem. Rev.* **2022**, *6*, 89–111; b) A. Piovano, E. Groppo, *Coord. Chem. Rev.* **2022**, *451*, 214258; c) J. R. Severn, J. C. Chadwick, R. Duchateau, N. Friederichs, *Chem. Rev.* **2005**, *105*, 4073–414.
[9] G. Zanchin, G. Leone, *Prog. Polym. Sci.* **2021**, *113*, 101342.
[10] a) C. Chen, *Nat. Chem. Rev.* **2018**, *2*, 6–14; b) M. Khoshsefat, Y. Ma, W.-H. Sun, *Coord. Chem. Rev.* **2021**, *434*, 213788; c) D. H. Camacho, Z. Guan, *Chem. Commun.* **2010**, *46*, 7879–7893; d) S. Mecking, *Angew. Chem. Int. Ed.* **2001**, *40*, 534–540; e) A. Nakamura, T. M. Anselment, J. Claverie, B. Goodall, R. F. Jordan, S. Mecking, B. Rieger, A. Sen, P. W. Van Leeuwen, K. Nozaki, *Acc. Chem. Res.* **2013**, *46*, 1438–1449.
[11] a) Z. Guan, P. Cotts, E. McCord, S. McLain, *Science* **1999**, *283*, 2059–2062; b) Y. Zhang, Z. Jian, *Macromolecules* **2020**, *53*, 8858–8866; c) L. Guo, S. Dai, X. Sui, C. Chen, *ACS Catal.* **2016**, *6*, 428–441; d) R. Wu, W. K. Wu, L. Stieglitz, S. Gaan, B. Rieger, M. Heuberger, *Coord. Chem. Rev.* **2023**, *474*, 214844; e) S. D. Ittel, L. K. Johnson, M. Brookhart, *Chem. Rev.* **2000**, *100*, 1169–1204; f) L. K. Johnson, C. M. Killian, M. Brookhart, *J. Am. Chem. Soc.* **1995**, *117*, 6414–6415; g) Z. Chen, M. Brookhart, *Acc. Chem. Res.* **2018**, *51*, 1831–1839; h) A. Nakamura, S. Ito, K. Nozaki, *Chem. Rev.* **2009**, *109*, 5215–5244; i) R. Wu, T. M. Lenz, L. Stieglitz, R. Galois, R. Zhao, P. Rupper, S. Lehner, M. Jovic, A. Neels, S. Gaan, B. Rieger, M. Heuberger, *J. Catal.* **2023**, *426*, 270–282.
[12] a) S. Dai, C. Chen, *Angew. Chem. Int. Ed.* **2020**, *59*, 14884–14890; b) J. P. McInnis, M. Delferro, T. J. Marks, *Acc. Chem. Res.* **2014**, *47*, 2545–2557; c) G. G. Hlatky, *Chem. Rev.* **2000**, *100*, 1347–1376; d) K. Patel, S. H. Chikkali, S. Sivaram, *Prog. Polym. Sci.* **2020**, *109*, 101290; e) C. Copéret, F. Allouche, K. W. Chan, M. P. Conley, M. F. Delley, A. Fedorov, I. B. Moroz, V. Mougel, M. Pucino, K. Searles, *Angew. Chem. Int. Ed.* **2018**, *57*, 6398–6440.
[13] a) S.-H. Wu, C.-Y. Mou, H.-P. Lin, *Chem. Soc. Rev.* **2013**, *42*, 3862–3875; b) W. Li, J. Liu, D. Zhao, *Nat. Rev. Mater.* **2016**, *1*, 1–17; c) D. Zhao, J. Feng, Q. Huo, N. Melosh, G. H. Fredrickson, B. F. Chmelka, G. D. Stucky, *Science* **1998**, *279*, 548–552; d) K. Lan, D. Zhao, *Nano Lett.* **2022**, *8*. 3177–3179.
[14] R. Wu, L. Stieglitz, S. Lehner, M. Jovic, D. Rentsch, A. Neels, S. Gaan, B. Rieger, M. Heuberger, *Eur. Polym. J.* **2023**, *186*, 111830.
[15] M. Patel, A. Kumar, S. K. Sahu, M. K. Singh, *Int. Res. J. Eng. Technol* **2020**, *7*, 201–204.
[16] S. Tanuma, C. J. Powell, D. R. Penn, *Surf. Interface Anal.* **1994**, *21*, 165–176.
[17] G. Beamson, D. Briggs, *Wiley: Chichester*, England, **1992**.
[18] D. R. Fahey, B. A. Baldwin, *Inorg. Chim. Acta* **1979**, *36*, 269–273.
[19] a) M. C. Biesinger, L. W. Lau, A. R. Gerson, R. S. C. Smart, *Phys. Chem. Chem. Phys.* **2012**, *14*, 2434–2442; b) M. C. Biesinger, B. P. Payne, A. P. Grosvenor, L. W. Lau, A. R. Gerson, R. S. C. Smart, *Appl. Surf. Sci.* **2011**, *257*, 2717–2730.
[20] M. Alexander, G. Thompson, G. Beamson, *Surf. Interface Anal.* **2000**, *29*, 468–477.
[21] E. Papirer, R. Lacroix, J.-B. Donnet, G. Nansé, P. Fioux, *Carbon* **1995**, *33*, 63–72.
[22] Y. K. Kim, in *Polyolefin Fibres*, Elsevier, **2017**, pp. 135–155.
[23] Z. Wang, Q. Liu, G. A. Solan, W.-H. Sun, *Coord. Chem. Rev.* **2017**, *350*, 68–83.
[24] H. Mu, G. Zhou, X. Hu, Z. Jian, *Coord. Chem. Rev.* **2021**, *435*, 213802.
[25] P. Rupper, M. Amberg, D. Hegemann, M. Heuberger, *Appl. Surf. Sci.* **2020**, *509*, 145362.

Manuscript received: October 11, 2023
Accepted manuscript online: January 16, 2024
Version of record online: February 1, 2024